

ORIGINAL ARTICLE

Open Access



# High-Speed Machining of Malleable Cast Iron by Various Cutting Tools Coated by Physical Vapor Deposition

Suyang Li<sup>1</sup>, Haisheng Lin<sup>1</sup>, Tingjie Zhang<sup>2</sup>, Jianbo Sui<sup>1</sup> and Chengyong Wang<sup>1\*</sup>

## Abstract

The coating material of a tool directly affects the efficiency and cost of machining malleable cast iron. However, the machining adaptability of various coating materials to malleable cast iron has been insufficiently researched. In this paper, turning tests were conducted on cemented carbide tools with different coatings (a thick TiN/TiAlN coating, a thin TiN/TiAlN coating, and a nanocomposite (nc) TiAlSiN coating). All coatings were applied by physical vapor deposition. In a comparative study of chip morphology, cutting force, cutting temperature, specific cutting energy, tool wear, and surface roughness, this study analyzed the cutting characteristics of the tools coated with various materials, and established the relationship between the cutting parameters and machining objectives. The results showed that in malleable cast iron machining, the coating material significantly affects the cutting performance of the tool. Among the three tools, the nc-TiAlSiN-coated carbide tool achieved the minimum cutting force, the lowest cutting temperature, least tool wear, longest tool life, and best surface quality. Moreover, in comparisons between cemented-carbide and compacted-graphite cast iron machined under the same conditions, the wear mechanism of the coated tools was found to depend on the cast iron being machined. Therefore, the performance requirements of a tool depend on multiple factors, and selecting an appropriately coated tool for a particular cast iron material is essential.

**Keywords:** Malleable cast iron, Tool-workpiece matching, Cemented carbide coated tool, PVD coating, Dry turning

## 1 Introduction

The graphite shape and matrix type of cast iron greatly influence the mechanical properties and machinability of the formed part [1–3]. Some commonly used cast irons are malleable cast iron (MCI), nodular cast iron (NCI), grey cast iron (GCI), and compacted cast iron (CGI). At present, the cutting tools for machine cast iron are mainly composed of polycrystalline cubic boron nitride (PCBN), ceramic, and cemented carbide [4]. Because the different machinabilities of different cast irons affect the tool life and tool wear in different ways, a suitable cutting tool must be found for each cast iron [5–9]. Reasonably

matching the tool and workpiece can effectively reduce the tool wear, lengthen the tool life, reduce the machining cost, improve the machining efficiency, and obtain excellent surface quality. The coating on the cutting tool also greatly affects the tool cutting performance. Toop-tong et al. [10] conducted dry turning tests on GCI, CGI, and NCI, and compared the tool wears of two cutting tools with different coatings: uncoated cemented carbide and multilayer-coated cemented carbide. They reported significantly lower flank wear on the multilayer-coated cemented carbide tool than on the uncoated cemented carbide tool; meanwhile, the flank wear on the uncoated cemented carbide tool was lower after cutting CGI and NCI than after cutting GCI.

NCI has a spherical graphite morphology, and exhibits high tensile strength, excellent ductility, high wear resistance, and elastic modulus. However, it is disadvantaged

\*Correspondence: cywang@gdut.edu.cn

<sup>1</sup> School of Electromechanical Engineering, Guangdong University of Technology, Guangzhou 510006, China  
Full list of author information is available at the end of the article

by poor heat dissipation. NCI is the typical constituent of internal combustion engines, automobile parts, and agricultural machinery. Yigit et al. [11] machined NCI using an uncoated cemented carbide tool and two kinds of coated cemented carbide tools with different coating thicknesses. The coating, TiCN + TiC + TiCN + Al<sub>2</sub>O<sub>3</sub> + TiN, was formed by high-temperature chemical deposition. During NCI processing at various cutting speeds, the thick cemented carbide tool with the TiCN + TiC + TiCN + Al<sub>2</sub>O<sub>3</sub> + TiN coating was the most suitable tool for turning NCI, especially in high-speed cutting. Martinez et al. [12] compared the tool wears of TiAlN and TiN coated carbide tools after cutting NCI. They found that the flank wear and built-up edge (BUE) were lower on the TiAlN coated tool than on the TiN coated tool, indicating that the TiAlN coated tool was more suitable for NCI machining. Jindal et al. [13] dry-turned NCI using cemented carbide tools coated with three different materials formed by physical vapor deposition (PVD): PVD TiN, PVD TiCN and PVD TiAlN. They found that the TiAlN coated tool delivered the best cutting performance, followed by the TiCN and TiN coated tools.

GCI has a mainly flaky graphite morphology, and is characterized by high brittleness and low tensile strength, but good thermal conductivity and high machinability. GCI is suitable for engine blocks, measurement equipment, the frames of machine tools, and other components requiring good shock absorption [14]. For GCI machining, a silicon nitride (Si<sub>3</sub>N<sub>4</sub>) ceramic tool is recommended. Owing to their high fracture toughness, high wear resistance and super chemical stabilities at evaluated temperature, Si<sub>3</sub>N<sub>4</sub> ceramic cutting tools show reliable cutting performance during the high speed machining of GCI [15–17]. Fiorini et al. [14] compared the tool wears, tool lifetimes, and tool failure mechanisms of uncoated and CVD TiN/Al<sub>2</sub>O<sub>3</sub>-coated Si<sub>3</sub>N<sub>4</sub> tools after GCI machining under continuous and intermittent cutting conditions. They attributed the high cutting performance of the TiN/Al<sub>2</sub>O<sub>3</sub>-coated tool to high wear resistance and toughness of the TiN/Al<sub>2</sub>O<sub>3</sub>. Long et al. [18] coated silicon-nitride ceramic cutting tools with PVD TiAlN and PVD CrAlN, and compared their performances with those of an uncoated silicon-nitride ceramic cutting tool in turning of GCI HT250. The cutting lives of their TiAlN and CrAlN coated tools were at least twice that of the uncoated tool.

CGI has a worm-like (vermicular) graphite morphology and demonstrates high strength, high toughness, and good plasticity and elongation, but poor machinability. CGI possesses similar mechanical properties to those of NCI, and is mainly used for automobile parts. Gabaldo et al. [19] analyzed the wear mechanisms and tool lifetimes of cutting tools fabricated from two kinds of

substrate materials (cemented carbide and ceramic Si<sub>3</sub>N<sub>4</sub>) during CGI finishing milling. Under the same cutting conditions, the life of the cemented carbide tool exceeded that of the ceramic tool, indicating that the cemented carbide tool is more suitable for CGI machining than the ceramic tool. Chen et al. [20] observed the wears of a PVD TiAlN coated carbide tool and an uncoated carbide tool in CGI milling. They found that the TiAlN coated tool lowered the average cutting temperature by approximately 40 °C from that of the uncoated tool, confirming that the PVD TiAlN coating material can effectively reduce the cutting temperature and prolong the tool life.

MCI exists in two forms: blackheart and whiteheart. This material has a flocculent graphite morphology and is characterized by high strength, high wear resistance, high toughness, and good plasticity. MCI is widely used for automobile and agricultural parts, pipe fittings, and valves, and is especially suitable for thin-walled parts with complex shapes and those bearing impact loads, such as axle bearings, track wheels, automobile crankshafts, and building hardware. However, most of the research has focused on NCI, GCI and CGI [21, 22], while MCI has been relatively neglected. Moreover, most of the existing research on MCI is limited to the castability of MCI [23]; few public reports have considered the machinability of MCI and the adaptability of MCI to cutting tools. Therefore, it is difficult to establish the cutting system of MCI, and its progression from coating material → preparation → cutting parameter optimization. To better understand the wear mechanism of coated tools, guide the processing technology of MCI, and support the selection of suitable coated tools and optimal parameters, one must study the machinability of MCI and match the material with a suitable cutting tool.

The present study evaluates the effectiveness of three cemented carbide coated tools with different coatings fabricated by PVD (a thick TiN/TiAlN coating, a thin TiN/TiAlN coating, and a nanocomposite (nc)-TiAlSiN coating) in MCI turning experiments. The influence of the coating materials on the cutting performances of the coated tools are investigated under various cutting conditions. After comparing the wear mechanisms of the coated tools in MCI and GCI machining, a suitable coating material for MCI machining is proposed.

## 2 Experimental Setup

### 2.1 Workpiece and Cutting Tools

The working specimens for the dry turning experiments were MCI (KTZ 700-02) round bars with a diameter and length of 100 mm and 150 mm, respectively. The average hardness and minimum tensile strength of MCI are 265 HV and 700 MPa, respectively. The chemical

compositions of MCI were detected by energy-dispersive spectroscopy (EDS) and are given in Table 1.

Three PVD-coated cemented carbide inserts were rigidly mounted in a tool holder with an ISO designation (CNMG120404-MF1 made by SEKO Corp., Switzerland). All tools had the same geometrical characteristics (rake angle = 25°, clearance angle = 0°, tool cutting edge angle = 95°, nose angle = 80°), and were recommended by the tool manufacturer for machining industrial cast irons. The detailed information of the coated tools is provided in Table 2. The coating structures and morphologies of the coated tools were observed by SEM, and the coating compositions were analyzed by EDS. The TiN (TiAlN) coating thicknesses of the thick and thin coated tools were 0.612 (2.53)  $\mu\text{m}$  and 0.467 (1.59)  $\mu\text{m}$ , respectively. The nc-TiAlSiN coating was applied in three layers with thicknesses of 0.612, 1.31, and 0.408  $\mu\text{m}$  from outside to inside. All cutting tools were formed on WC + Co substrate. The grain size was finest in the nc-TiAlSiN coated tool, intermediate in the thick TiN/TiAlN coated tool, and coarsest in the thin TiN/TiAlN coated tool. The Vickers hardness and roughness values of the coated tools were measured by an HXD-1000TM/LCD digital microhardness tester and a MarSurf meter XT20, respectively. The hardness value was highest in the nc-TiAlSiN coated tool, intermediate in the thin TiN/TiAlN coated tool, and lowest in the thick TiN/TiAlN coated tool. The roughness values were lower in the thin TiN/TiAlN coated and nc-TiAlSiN coated tools than in the thick TiN/TiAlN.

## 2.2 Measuring Equipment

Cylindrical turning experiments were performed on a CAK3665NJ NC lathe made by China Shenyang Machine Tool CNC Co., Ltd. The tools' responses to three-dimensional forces (axial feed force  $F_x$ , radial feed force  $F_y$  and tangential feed force  $F_z$ ) were measured by a piezo-electric dynamometer (Kistler 9129AA, Kistler Instrument®) linked to a Kistler charge amplifier (Kistler 5080A1030001, Kistler Instrument®). These analog signals were transformed into digital signals by a DAQ Card (Model DEWE 43V). The cutting temperatures during the experiments were measured and recorded by a thermal infrared imager (TVS-500EX, NEC®, NEC Company, Japan). The thermal infrared equipment was calibrated by measuring the temperature of the workpiece while heating it to a set temperature in a chamber electric furnace. The surface roughness was measured by

a portable roughness meter (TR2000, Beijing Times Co., Ltd., China). The chip morphology and tool wear were observed under an optical microscope (OLYMPUS SZ61, Japan). An average flank wear of  $VB = 0.3$  mm was used as the tool-wear criterion. The tool wear was observed by scanning electron microscopy (SEM, S-3400N-II, Hitachi, Japan) and energy dispersive spectroscopy (EDS, Zeiss Group®). The cutting experimental system is depicted in Figure 1.

## 2.3 Dry Turning Experiments

The effect of the coating materials on the cutting performance of the coated tools was evaluated in dry turning experiments on a CAK3665NJ NC lathe. The evaluation variables (cutting speed  $v$ , depth of cut  $a_p$  and feed rate  $f$ ) and their values are shown in Table 3. All experiments were carried out under dry cutting conditions. The effects of the various cutting parameters on the cutting force and cutting temperature of the coated tools were examined during MCI turning. The cutting parameters of MCI were constant and set to  $v = 150$  m/min,  $f = 0.15$  mm/rev and  $a_p = 0.9$  mm. Each turning experiment was performed thrice under the same cutting conditions, and the results were averaged to give the final result. The total number of experiments was 45. The chip morphology, cutting force, cutting temperature, tool wear, and surface roughness were measured.

## 3 Experimental Results

### 3.1 Characteristics of the Cutting Process

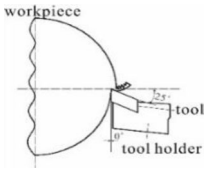
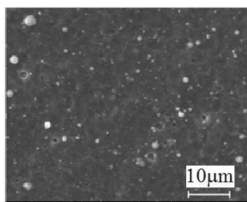
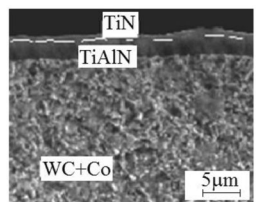
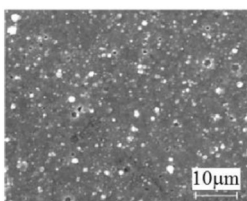
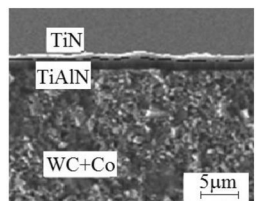
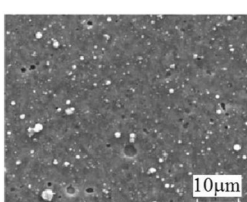
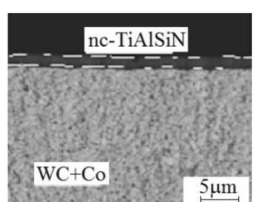
#### 3.1.1 Chip Morphology

Figure 2 depicts the chip morphologies of three kinds of coated tools under different cutting parameters. Obviously, the cutting parameters largely influenced the chip morphology. As shown in Figure 2a–c, keeping the cutting depth unchanged, when the three coated tool were respectively applied at  $f = 0.15$  mm/rev and low cutting speed, most of the chip morphologies were continuous C-shaped pieces with sawtooth patterns, indicating a plastic character. At higher cutting speeds, the chips transformed from C-shaped to arc-shaped ones, and the chip length became shorter. On the other hand, keeping the cutting speed unchanged, as the cutting depth increased, the radius of the circular arc of the C-shaped chips increased gradually, showing a trend of “straightening”, the chip length and width increased, and the serration became more obvious. This behavior can be

**Table 1** Chemical compositions of MCI

Element	C	Si	Mn	S	P	Fe
Amount (%)	6.00–7.53	2.4–3.08	0.4–0.5	$\leq 0.20$	$\leq 0.1$	Balance

**Table 2** Details of the investigated coated tools

Tool holder type: DCLNR225M12				
				
No.	Tool type	Thickness of coatings	Hardness	Roughness
1	CP500 PVD coating Thick TiN/TiAlN WC substrate	TiN 0.612 μm TiAlN 2.53 μm	2785 HV <sub>50gf</sub>	0.380 μm
	 	Tool surface SEM Cross section morphology of coatings		
2	TS2000 PVD coating Thin TiN/TiAlN WC substrate	TiN 0.467 μm TiAlN 1.59 μm	2864 HV <sub>50gf</sub>	0.266 μm
	 	Tool surface SEM Cross section morphology of coatings		
3	TH1000 PVD coating nc-TiAlSiN WC substrate	nc-TiAlSiN 0.612 μm 1.31 μm 0.408 μm	3668 HV <sub>50gf</sub>	0.268 μm
	 	Tool surface SEM Cross section morphology of coatings		

explained by the increased force and power of the cutting at greater cutting depths, which raised the cutting temperature and the severity of the adiabatic shear.

As shown in Figure 2d–f, at low cutting speed and low feed rate (i.e.,  $v = 50$  m/min,  $f = 0.05$  mm/rev), most of the chip morphologies produced by the three coated tools were continuous C shape or spiral tube shape. Increasing the cutting speed and feed rate changed the C-shaped chips to arc-shaped ones. At higher cutting speeds, especially when  $v \geq 150$  m/min, the chips fragmented and the fragments widths increased with the increasing feed rate.

Comparing Figure 2a–f, it is found that no matter which coated tool was used, the change trends of chip morphologies with cutting parameters for the three coated tools were almost the same, indicating that chip morphology was mainly related to cutting parameters, but rarely to coating materials.

### 3.1.2 Cutting Force

Figure 3 plots the resultant cutting forces as functions of the cutting parameters for the three carbide coated tools. The coating materials significantly influenced the cutting forces. The observed trends can arise from the different friction coefficients between the various coating materials and their workpieces, which directly lead to inconsistent cutting forces [24]. Meanwhile, the different heat conductions in the various coating materials during machining indirectly alter the cutting forces, as reported in our previous research [25]. Among the three coated tools, the nc-TiAlSiN coated tool exerted the lowest cutting force under the same cutting conditions. This result may be explained by the small grain size in the nc-TiAlSiN coating material. Owing to its nanocomposite structure, nc-Ti<sub>1-x</sub>Al<sub>x</sub>N/a-Si<sub>3</sub>N<sub>4</sub> achieved better hardness, surface finish, and oxidation resistance than the other coated tools [26]. Therefore, nc-TiAlSiN coated tool exhibited good friction and wear resistance, effectively reducing the cutting force.

The cutting speed less affected the cutting force than the cutting depth and feed rate (Figure 3a). For each cutting parameter, the trend in the resultant cutting force was more pronounced in the thick TiN/TiAlN coated tool than in the thin TiN/TiAlN and nc-TiAlSiN coated tools. As shown in Figure 3a, as the cutting speed ranged from 50 to 250 m/min, the resultant cutting force of the thick TiN/TiAlN coated tool gradually trended upward, and the rising trend decreased slightly at  $v > 150$  m/min, but those of the thin TiN/TiAlN and nc-TiAlSiN coated tools stabilized at higher cutting speeds. Similar results have been reported by Song [27] and Silva [28]. This outcome might manifest from material deformation (which is slow at lower cutting speeds), and dynamic strain hardening and strain rate hardening (which increases the cutting

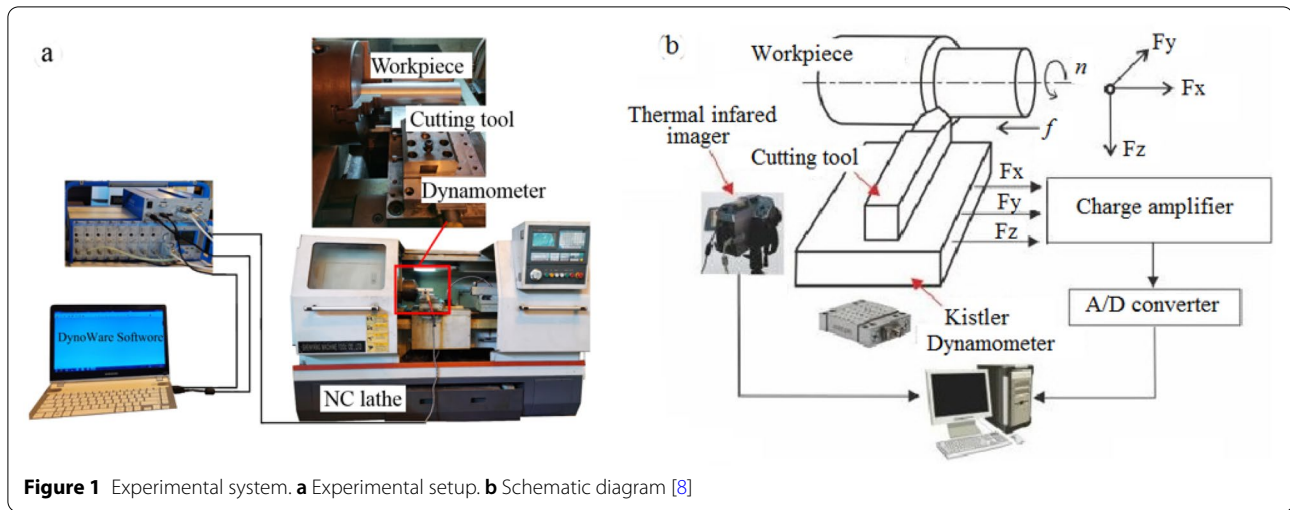


**Figure 1** Experimental system. **a** Experimental setup. **b** Schematic diagram [8]

**Table 3** Experimental parameters in dry turning of MCI

Cutting parameters	Cutting speed, $v$ (m/min)	Feed rate, $f$ (mm/rev)	Depth of cut, $a_p$ (mm)
Cutting speed $v$	50, 100, 150, 200, 250	0.2	0.9
Depth of cut $a_p$	150	0.15	0.3, 0.6, 0.9, 1.2, 1.5
Feed rate $f$	150	0.05, 0.1, 0.15, 0.2, 0.25	0.9
Cutting tools	PVD thick TiN/TiAlN coated tool, PVD thin TiN/TiAlN coated tool, PVD nc-TiAlSiN coated tool		

force). At higher cutting speeds, thermal softening plays a more dominant role at elevated temperature; consequently, the shear strength of the material was reduced, and the cutting force reduced accordingly.

The cutting depth and feed rate more significantly affected the cutting force than cutting speed, as shown in panels (b) and (c) of Figure 3. Similar conclusions were reported elsewhere [29]. The resultant force increased almost linearly with both cutting depth and feed rate. Incrementing these variables increased the material removal volume, thereby increasing the required cutting power and also the cutting force. Therefore, higher cutting speed, lower depth of cut, and lower feed rate resulted in lower cutting force.

MCI, CGI and NCI elicit different responses of the cutting force to various cutting parameters. Ding [30] reported that in the 71–210 m/min range of cutting speeds, the cutting force of dry turning by a CGI  $\text{Al}_2\text{O}_3/\text{TiCN}$  carbide coated tool decreased slightly with increasing cutting speed. Yigit et al. [31] reported similar results for dry turning of NCI with coated and uncoated tools. However, Katuku et al. [32] found that during dry turning of austempered ductile iron with a PCBN tool, increasing the cutting speed induced a rapid initial decrease in cutting force, followed by a slow increased. Various cast iron materials and cutting tools thus exert different effects

on the cutting force, and suitable cutting tools must be matched to different workpiece materials.

### 3.1.3 Effect of Coated Tools on Specific Cutting Energy

In dry turning, the specific cutting energy (SCE) refers to the cutting energy consumed per unit amount of material removal volume, which depends upon the consumed cutting power ( $P_c$ , in W) and the material removal rate ( $MRR$ , in  $\text{mm}^3/\text{s}$ ) as shown in Eq. (1) [33, 34]:

$$E_{\text{specific}} = \frac{P_c}{MRR}, \quad (1a)$$

$$P_c = \frac{F_c v}{60}, \quad (1b)$$

$$MRR = \frac{1000v \cdot a_p \cdot f}{60}, \quad (1c)$$

where  $E_{\text{specific}}$  is the specific cutting energy ( $\text{J}/\text{mm}^3$ ), and  $F_c$  is the tangential cutting force (N).

Figure 4 shows the specific cutting energy consumed by different coated carbide tools in dry turning of MCI. The cutting speed exerted an insignificant effect on the specific cutting energy, and can be increased in accordance with the machine tool power. Increasing

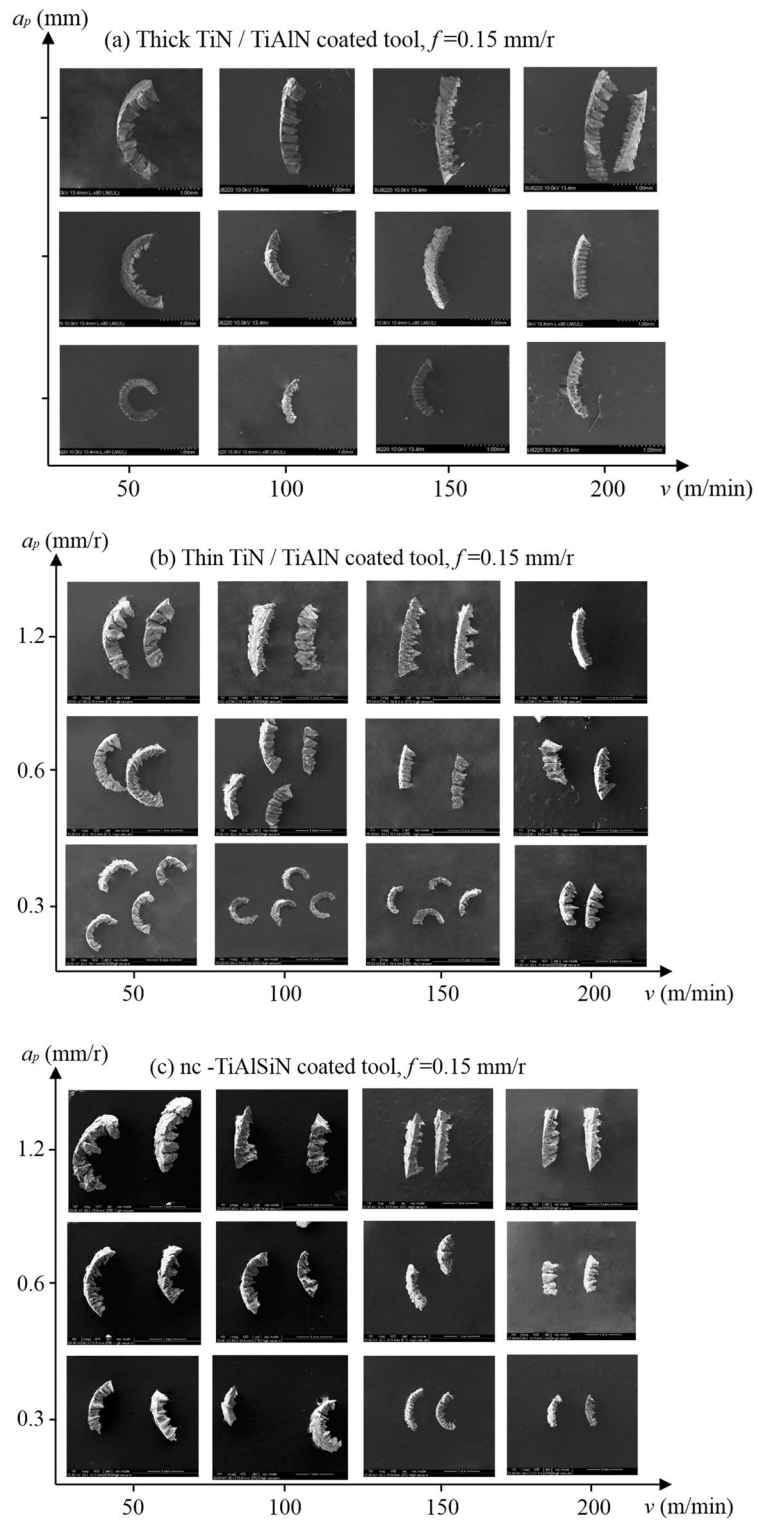


**Figure 2** Chip morphologies of the three PVD coated tools under various cutting parameters in dry turning of MCl

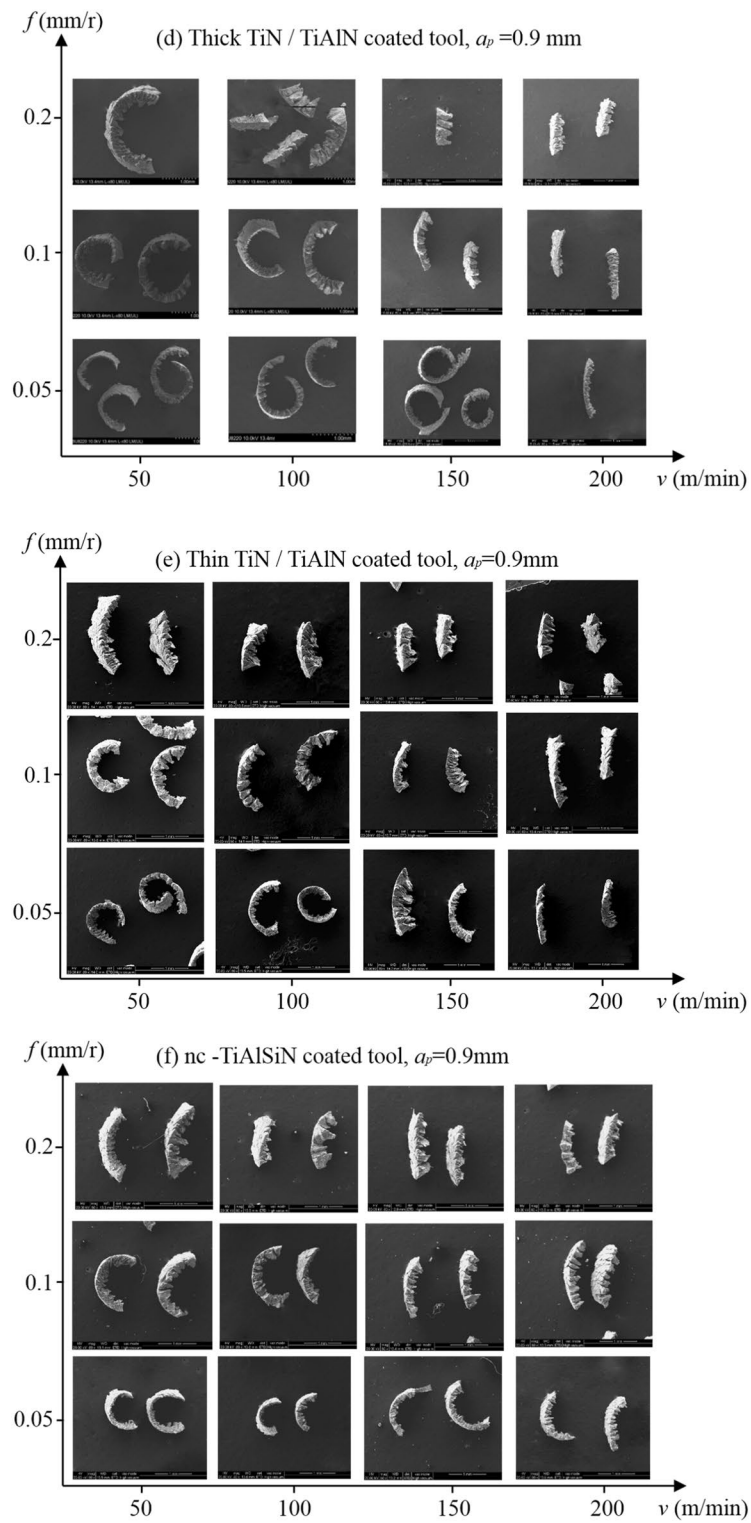
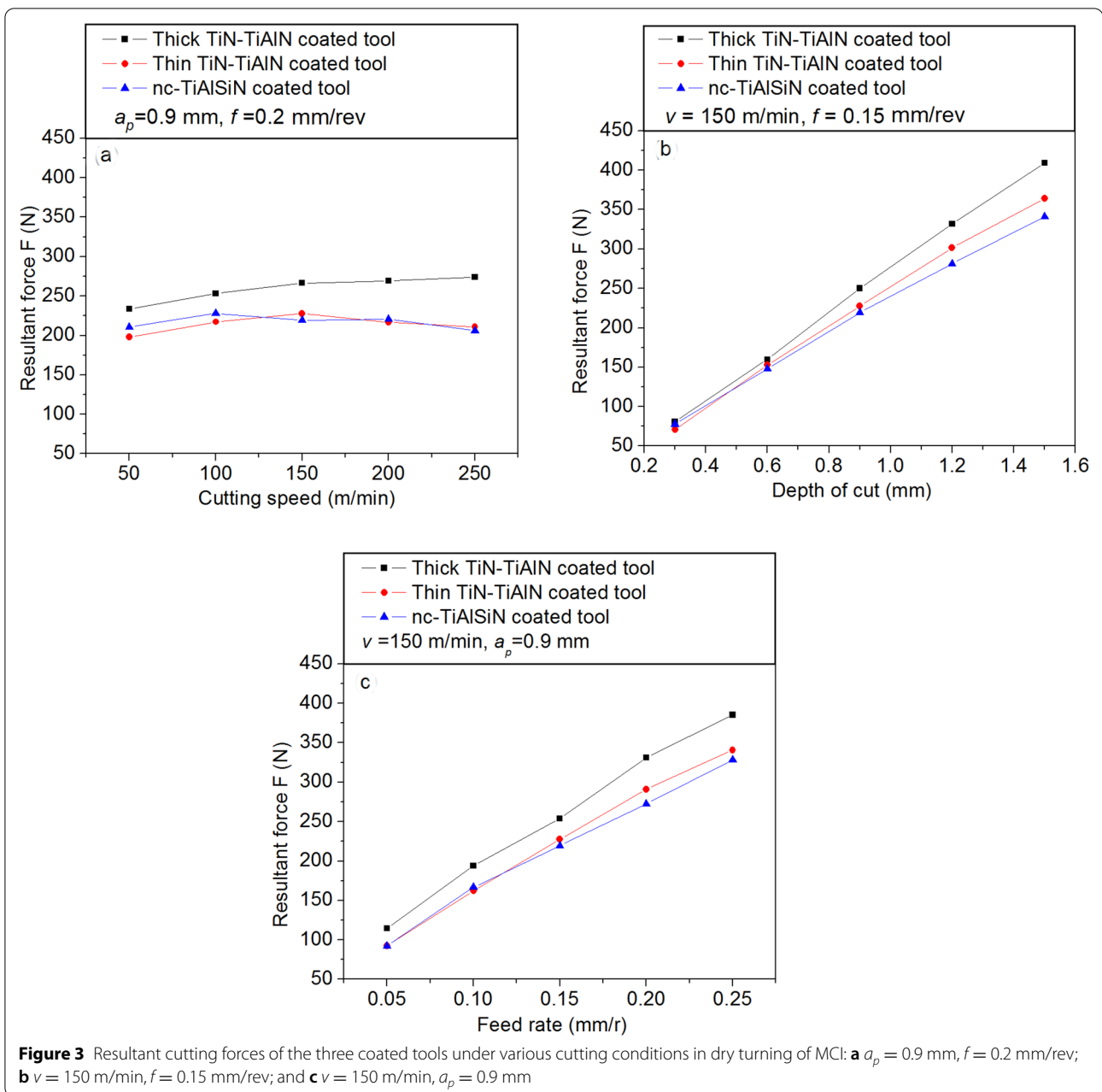


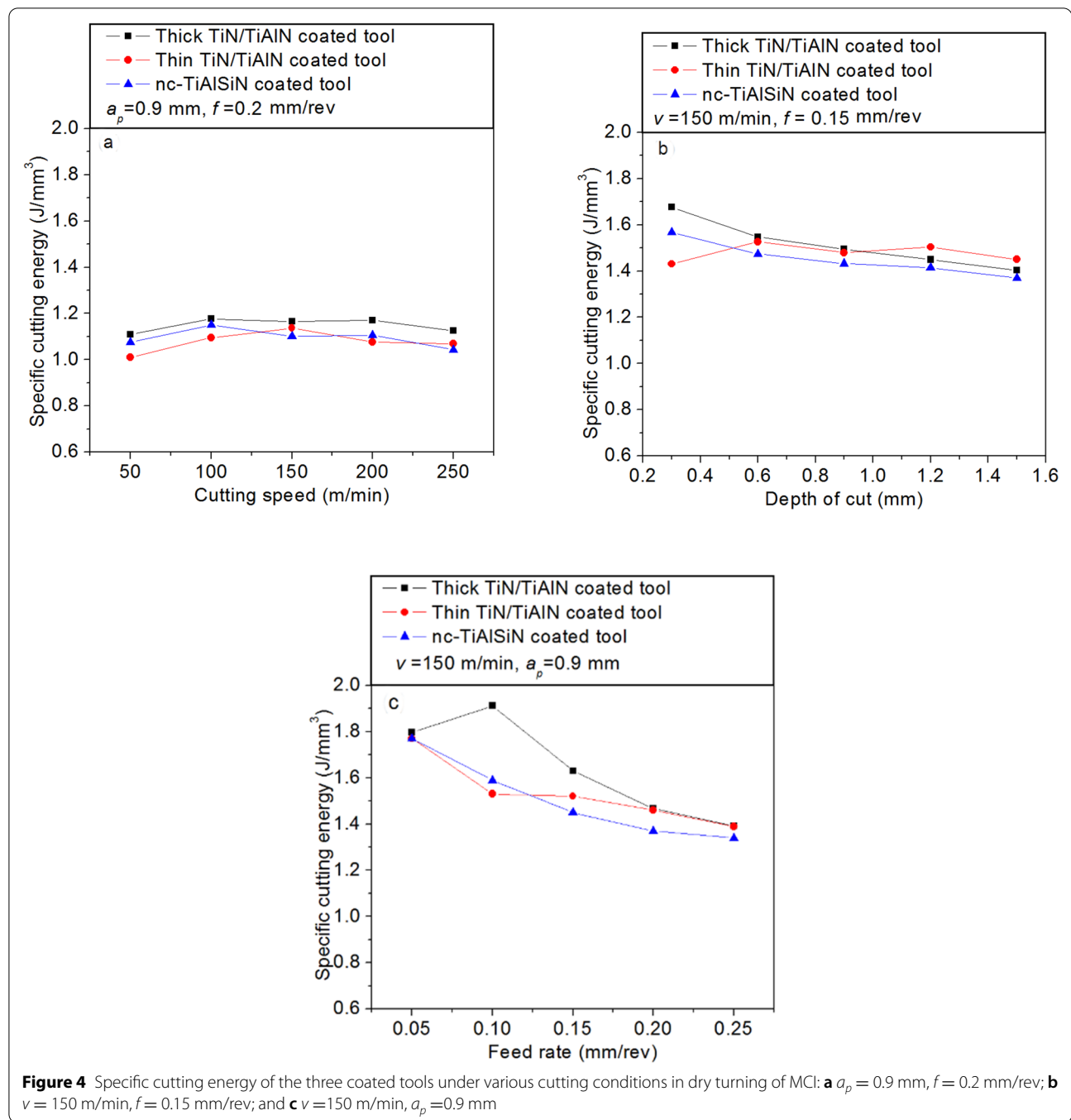
Figure 2 continued



the cutting depth gradually decreased the specific cutting energy; in the 0.3–1.5 mm range of cutting depths, a large cutting depth is preferred for energy saving. The feed rate also affected the specific cutting energy. Within the 0.05–0.25 mm/rev range of feed rates, the specific cutting energy of the thick TiN/TiAlN coated carbide tool was maximized. However, the specific cutting energy of the thin TiN/TiAlN and nc-TiAlSiN coated tools decreased with increasing feed rate. Therefore, to conserve energy use by these

tools, the specific cutting energy can be lowered by enlarging the cutting parameters.

The cutting conditions also greatly influence the temperature of the cutting zone. As the temperature increases, the yield strength and strain hardening effect of the workpiece material decrease, thereby reducing the specific cutting energy. Among the three coated tools, the nc-TiAlSiN coated tool consumed the lowest specific cutting energy, indicating that this tool consumed the lowest energy per unit cutting amount.



### 3.1.4 Cutting Temperature

The cutting temperature refers to the average temperature of the contact area between the chips and the rake face of the coated tools in the cutting zone. During dry turning of MCI by the present tools, this temperature was measured by a thermal infrared imager (TVS-500EX, NEC®, NEC Company, Japan), as shown in Figure 1. A thermal image during the temperature

measurement process is depicted in Figure 5, and the measured results are shown in Figure 6. Under the same cutting conditions, the coating material greatly influenced the average interface temperature. Among the three coated tools, the average interface temperature was highest for the nc-TiAlSiN coated tool, second-highest for the thick TiN/TiAlN coated tool, and lowest for the thin TiN/TiAlN coated tool. This finding

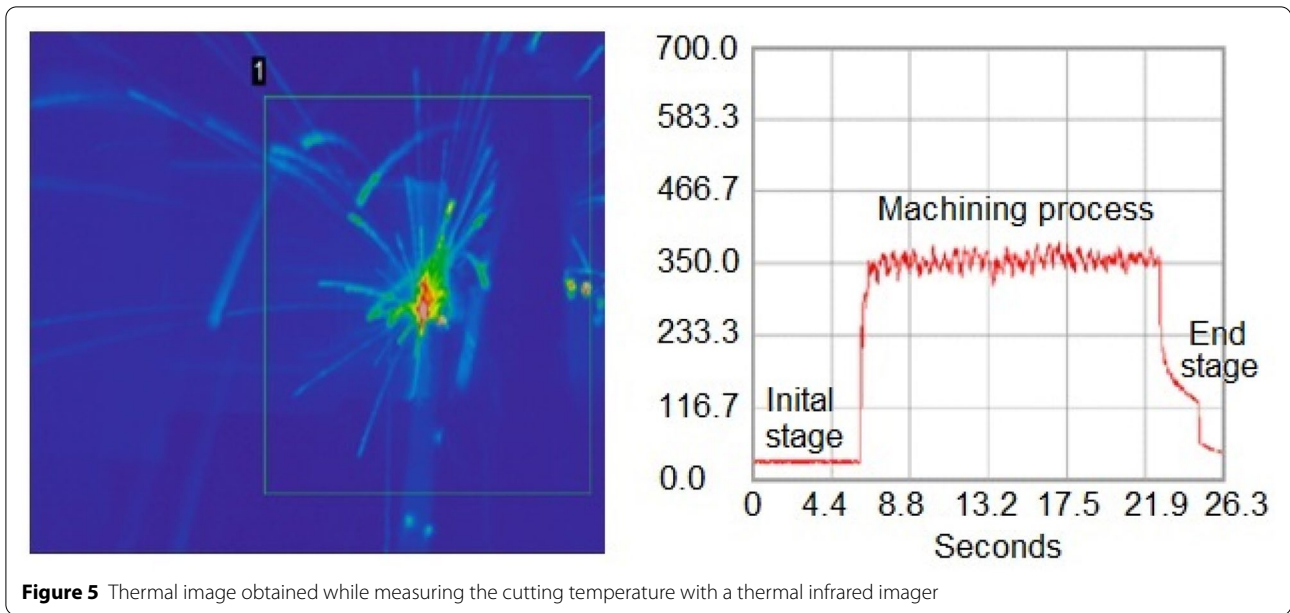


**Figure 5** Thermal image obtained while measuring the cutting temperature with a thermal infrared imager

can be explained by the influence of coating materials on the cutting heat distribution.

Most of the generated cutting heat was removed by the chips, and the remainder was dissipated by the workpiece, cutting tool, and surrounding environment. The cutting-heat distribution is related to the thermal conductivity of the coated tools. Although thermal conductivity is difficult to measure in multi-layered coating materials, it was assumed to be equivalent to that of stacked single-layer materials as described in Refs. [35, 36]. The formula is given by

$$\lambda_{eq} = \frac{\sum_{i=1}^n t_i}{\frac{t_1}{\lambda_1} + \frac{t_2}{\lambda_2} + \dots + \frac{t_n}{\lambda_n}} \quad (2)$$

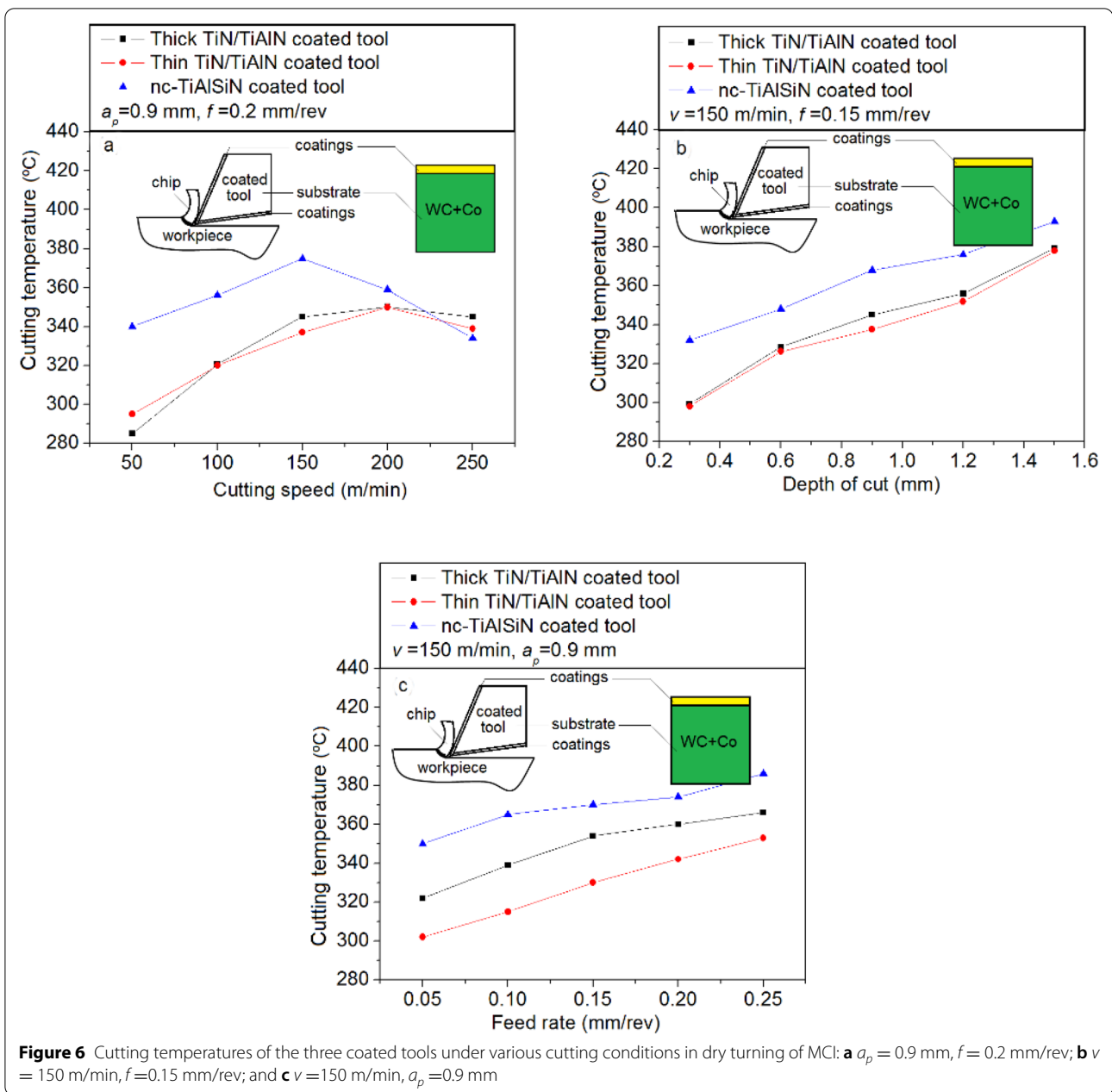
where  $\lambda_{eq}$  is the equivalent thermal conductivity of the multilayer coating, and  $\lambda_i$  and  $t_i$  denote the thermal conductivity and thickness, respectively, of single-layer coating  $i$  ( $i = 1, 2, \dots, n$ ).  $\sum t_i$  is the total thickness of the multilayer coating. From Eq. (2), the equivalent thermal conductivities of the thick TiN/TiAlN, thin TiN/TiAlN, and nc-TiAlSiN coatings at 300°C were computed as 15.07, 15.26, and 3.7 W·m<sup>-1</sup>·K<sup>-1</sup>, respectively. Obviously, the nc-TiAlSiN coating material had the lowest thermal conductivity, meaning that it transferred the lowest cutting heat to the tool substrate. Therefore, most of the cutting heat from this tool flowed to the chips, and the interface temperature of the tool–chip contact was higher than for the other tools. Similar investigations were conducted by Grzesik [37] and Zhang [38].

The effect of cutting speed on the cutting temperature is illustrated in Figure 6a. The cutting temperature increased up to some value of the cutting speed, and decreased at faster speeds. Increasing the cutting speed increased the friction in the contact area between the chip and the tool rake face, thereby increasing the friction heat. The amount of metal removal per unit time also increased, increasing the power consumption and cutting heat, and hence the cutting temperature. When the cutting speed reached a certain value, thermal softening of the metal played a leading role, and the heat dissipation area increased, thereby reducing the cutting temperature. Panels (b) and (c) of Figure 6 depict the cutting temperature dependences on cutting depth and feed rate, respectively. Increasing the cutting depth and feed rate increased the metal removal rate and hence the cutting temperature.

### 3.2 Cutting Tool Wear

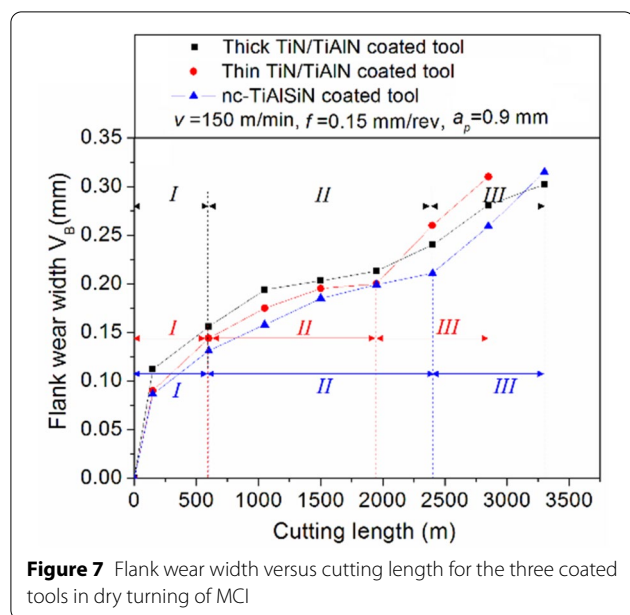
#### 3.2.1 Effects of Cutting Tools on Flank Wear

The tool wear rate during turning of MC was evaluated from the flank wear width, as shown in Figure 7. The tool-wear curves typify the curves obtained during normal metal cutting, such as the high-speed machining of hardened steel [39, 40]. As seen in Figure 7, increasing the cutting length increased the wear value of all coated tools. Tool wear can be divided into three stages: (I) initial wear, (II) stable wear, and (III) severe wear. The initial wear of the three coated tools occurred in the 0–600 m range of cutting lengths, and was characterized by a



sharp rise in wear width. During the stable wear stage, the cutting length was longer in the thick TiN/TiAlN and nc-TiAlSiN coated tools than in the thin TiN/TiAlN coated tool. When the cutting length exceeded 1950 m, the thin TiN/TiAlN coated tool entered the severe wear stage, while the thick TiN/TiAlN and nc-TiAlSiN coated tools remained in the stable stage. These tools entered the severe wear stage at cutting lengths beyond 2400 m. Moreover, during the severe wear stage, the thick TiN/TiAlN coated tool wore more safely than the thin TiN/TiAlN coated tool.

The thick TiN/TiAlN coated, thin TiN/TiAlN coated, and nc-TiAlSiN coated tools reached the tool wear criterion ( $VB = 0.3$  mm) at 3300 m, 2850 m and 3300 m, respectively. Obviously, that nc-TiAlSiN coated tool achieved the minimum flank wear and longest tool life among the tools. This result can be explained by the high hardness, good surface finish, low thermal conductivity, and good oxidation resistance of the nc-TiAlSiN coated tool [41]. These properties reduce the friction and hence the tool wear. Owing to the low flank wear, the nc-TiAlSiN coated tool achieved the best surface quality of the



workpiece (Figure 10) throughout the cutting process. However, during the later stage of rapid wear, the thick TiN/TiAlN coated tool wore more slowly than the other tools. Therefore, when the wear value of the flank face reached the tool wear criterion, the wear degree was slighter on the thick TiN /TiAlN coated tool than on the other tools, and the life of this tool was the longest, as verified in Figure 8. To maximize the tool wear and workpiece surface quality, the nc-TiAlSiN coated tool is the best choice, followed by the thick TiN/TiAlN coated tool. The thin TiN/TiAlN coated tool is a poor choice for these purposes.

### 3.2.2 Tool Wear Mechanism

Under the cutting conditions of  $v=150$  m/min,  $a_p=0.9$  mm, and  $f=0.15$  mm/rev, Figure 8 shows the wear morphologies of the three coated tools at their longest cutting distances. On the flank face of the thick TiN/TiAlN coated tool, the wear band was uniform and thick adhesion and some abrasive particles were found near the cutting edge, indicating an abrasive wear mechanism on the flank face. An EDS analysis of point A on the flank face revealed a large number of Fe, O and Al elements, with dominant Fe in the MCI and dominant Al in the coating element. This result indicates that the thick TiN/TiAlN coated tool was mainly subjected to adhesive and oxidation wear. An EDS analysis of point B in the exposed area of the rake face (where the coating material was peeled off) confirmed that the main elements of the tool substrate (W and Co) had been completely removed.

Being formed with the same coating materials, the thin TiN/TiAlN coated tool was subjected to the same wear

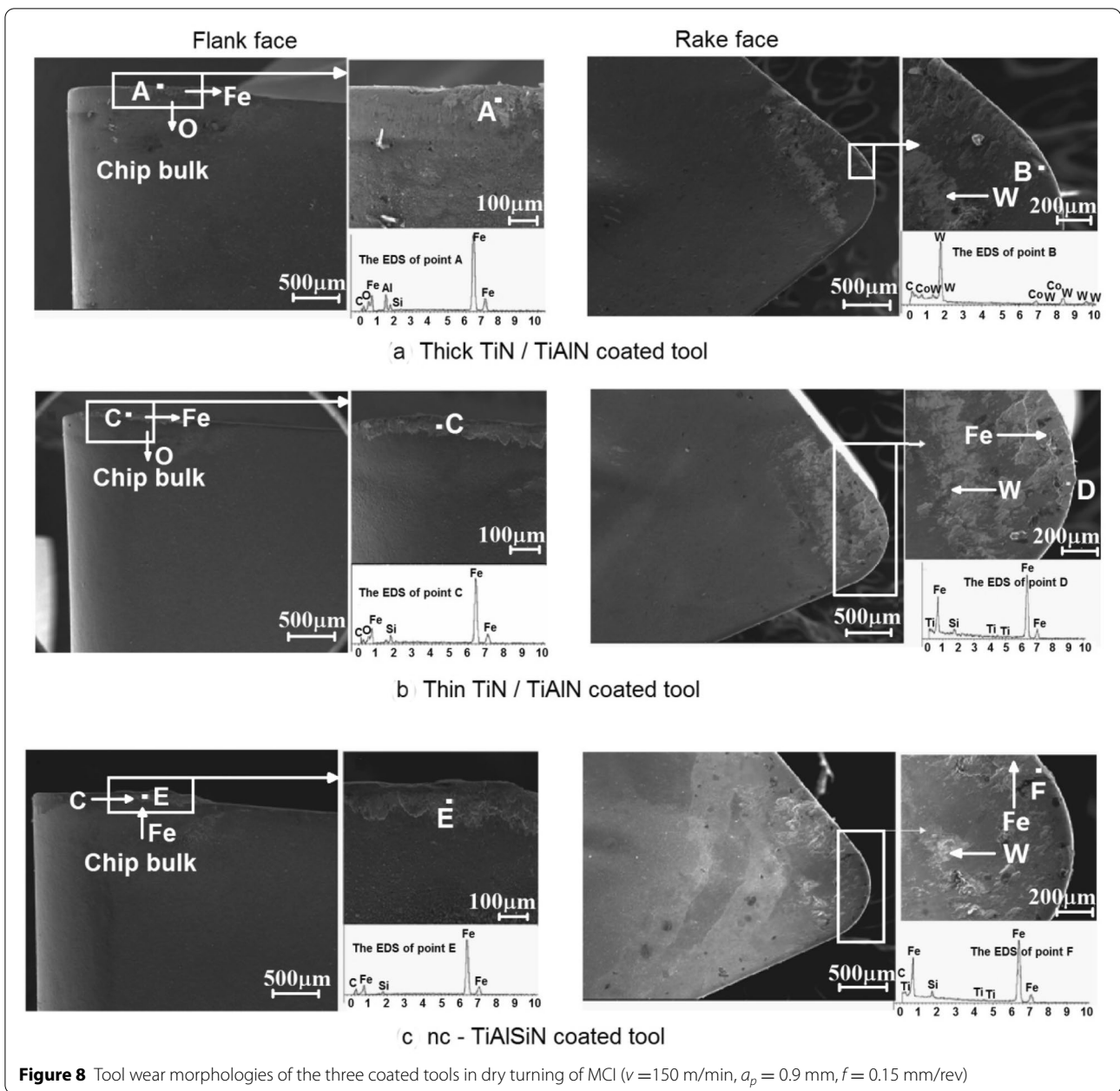
mechanisms as the thick TiN/TiAlN coated tool, but the adhesive wear was more severe on the thin TiN/TiAlN coated tool than on its thick counterpart, and abrasive particles appeared on the flank and rake faces of the thin-coated specimen (see Figure 8b). An EDS analysis of Point C on the tool's flank face revealed many Fe and O elements, but at point D on the rake face, the dominant element was Fe. According to this observation, the thin TiN/TiAlN coated tool in dry turning of MCI was subjected mainly to adhesive wear, accompanied by oxidation wear.

The nc-TiAlSiN coated tool featured a uniform wear band with a large amount of adhesion near the cutting edge (Figure 8c). The presence of abrasive particles on the flank face indicates that abrasive wear occurred there. An EDS analysis of the adhesion revealed dominant Fe at Point E on the flank face and dominant C at Point F on the rake face. As both elements are the main components of the workpiece, this result indicates that the workpiece material bonded with the cutting tool during the machining process. Therefore, the nc-TiAlSiN coated tool was subjected mainly to adhesive wear, accompanied by abrasive wear.

The thick TiN/TiAlN coated tool presented the lowest wear degree on the rake and flank faces, followed by the nc-TiAlSiN coated tool and the thin TiN/TiAlN coated tool. A thicker coating of the same material will better protect the tool than a thin coating, so a higher wear resistance of the thicker-coated tool is expected. Especially in the severe wear stage (see Figure 7), the wear rate of the thick TiN/TiAlN coated tool was the slowest among the examined tools, so this tool exhibited the slightest wear degree at the wear criterion. Although the nc-TiAlSiN coated tool required the highest cutting temperature (Figure 6), the amount of material adhered from the MCI (mainly Fe) was significantly lower on this tool than on the other TiN/TiAlN coated tools, indicating that the nc-TiAlSiN coating has low chemical affinity to MCI. Low adhesion to the machined material improves the surface roughness, as verified in Figures 10 and 11. The Si additive transforms the TiAlN coating to an amorphous  $\text{Si}_3\text{N}_4$  nano-composite structure surrounded by nano TiN. Such grain refinement effectively improves the hardness, wear resistance, and temperature oxidation resistance of the coated tool [26, 42].

### 3.2.3 Comparison of Tool Wear in MCI and CGI Turning

The different mechanical properties of MCI and CGI are attributable to their different graphite morphologies. To study the machining adaptability of the three coated tools to different workpiece materials, the tool wear in dry turning of MCI was compared with that of CGI as a

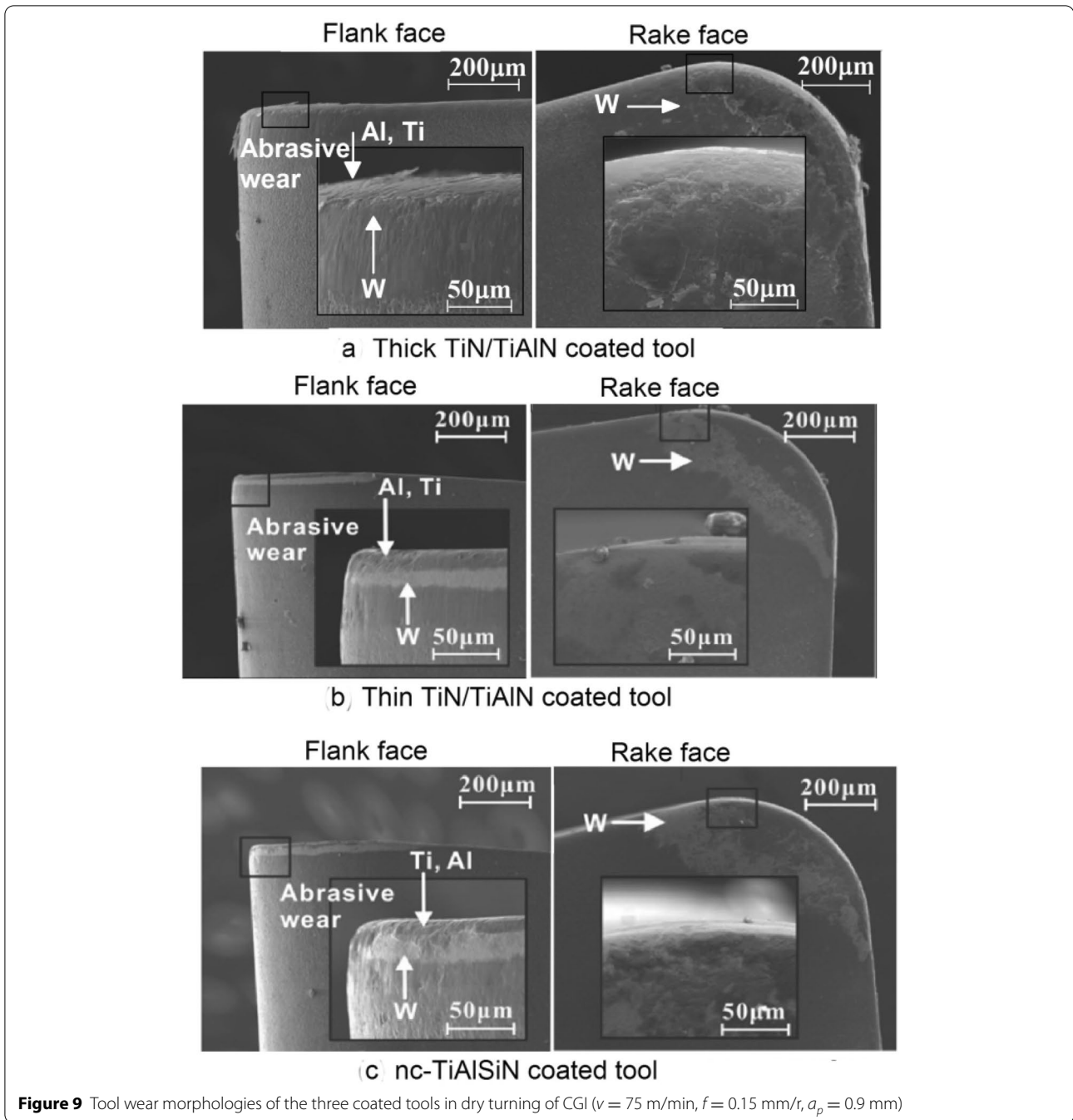


reference material. The CGI turning was performed at a reduced cutting speed to mitigate abnormal tool damage.

The predominant wear mechanisms of the three coated tools differed between CGI and MCI turning (c.f. Figures 8 and 9; see also Table 4). In GCI turning, only a small amount of Fe was adhered near the cutting zone. Large substrate- exposed areas (predominantly W) appeared on the rake and flank faces of all coated tools, indicating that all coatings were worn. The three tools were mainly subjected to abrasive wear, which may be attributed to the hardness of the particles

in CGI [43]. In addition, the non-uniform structure of CGI will mechanically impact on the tool during the cutting process.

Notably, the material properties altered the wear mechanisms of the tools; subsequently, different cast irons (i.e. MCI and CGI) require different tool properties. Based on the above analysis, CGI requires a tool with high hardness and high mechanical impact resistance, whereas MCI turning requires a tool with low affinity and low friction performance.



### 3.3 Surface Roughness

As the cutting length increased throughout the MCI cutting process, the surface roughness of the machined workpiece surface followed the same trend as the tool wear (Figure 7). More specifically, the surface roughness continuously increased with cutting length, as shown in Figure 10. Similar behavior was reported by Koshy et al. [41]. One may easily conclude that tool wear affects the

surface roughness. However, the work in [44] concluded otherwise. The authors of [44] presented a zig-zag curve of surface roughness along the cutting length of nodular cast iron. Figure 10 associates a smaller flank wear with lower surface roughness. In our study, the nc-TiAlSiN coated tool exhibited the lowest surface roughness owing to its low cutting force and minimal tool wear (recall that

**Table 4** Comparison of tool wear mechanisms in MCI and CGI turning

Workpiece material	Material property	Predominant tool wear mechanism		
		Thick TiN/TiAlN coated tool	Thin TiN/TiAlN coated tool	nc-TiAlSiN coated tool
MCI	Higher ductility, higher toughness, uniformity	Adhesive wear	Adhesive wear	Adhesive wear
CGI	Higher strength, higher hardness, non-uniformity	Abrasive wear	Abrasive wear	Abrasive wear

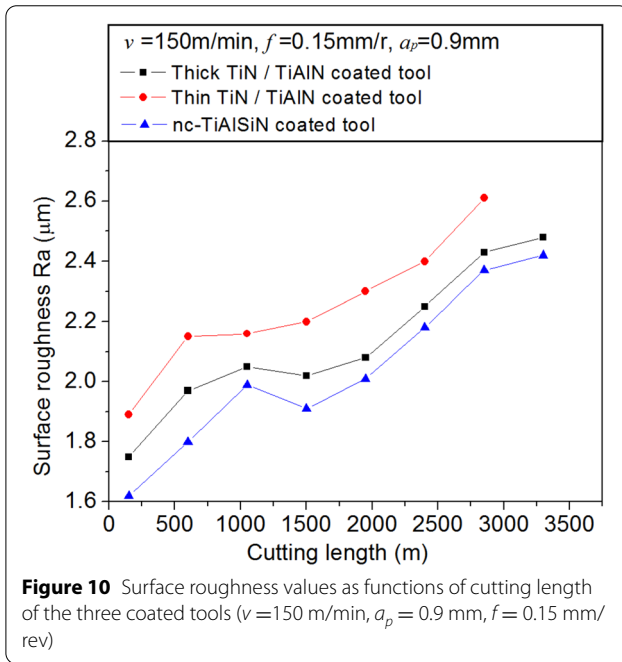


**Figure 10** Surface roughness values as functions of cutting length of the three coated tools ( $v=150$  m/min,  $a_p=0.9$  mm,  $f=0.15$  mm/rev)

both properties improved the surface quality of the nc-TiAlSiN coated tool over those of the other tools).

Figure 11 plots the surface roughness values of the three carbide coated tools as functions of the three cutting parameters at the longest cutting distance. The surface roughnesses of all tools decreased with increasing cutting speed at  $a_p = 0.9$  mm and  $f = 0.15$  mm/rev, implying that the surface finish of the workpiece improved with increasing cutting speed (see Figure 11a). However, increasing the feed rate while fixing the other cutting parameters elicited a sharp increase in surface roughness (Figure 11b). Similar behavior was observed by Patel et al. [45]. Both the cutting speed and feed rate exerted a much greater influence on surface roughness than cutting depth. Increasing the depth of cut initially decreased and thereafter increased the surface roughness of all cutting tools. At  $v = 150$  m/min and  $f = 0.15$  mm/rev, the surface roughnesses of the thin TiN/TiAlN coated and nc-TiAlSiN coated tools were minimized at  $a_p$

$= 0.9$  mm, whereas that of the thick TiN/TiAlN coated tool was lowest at  $a_p = 1.2$  mm (see Figure 11c).

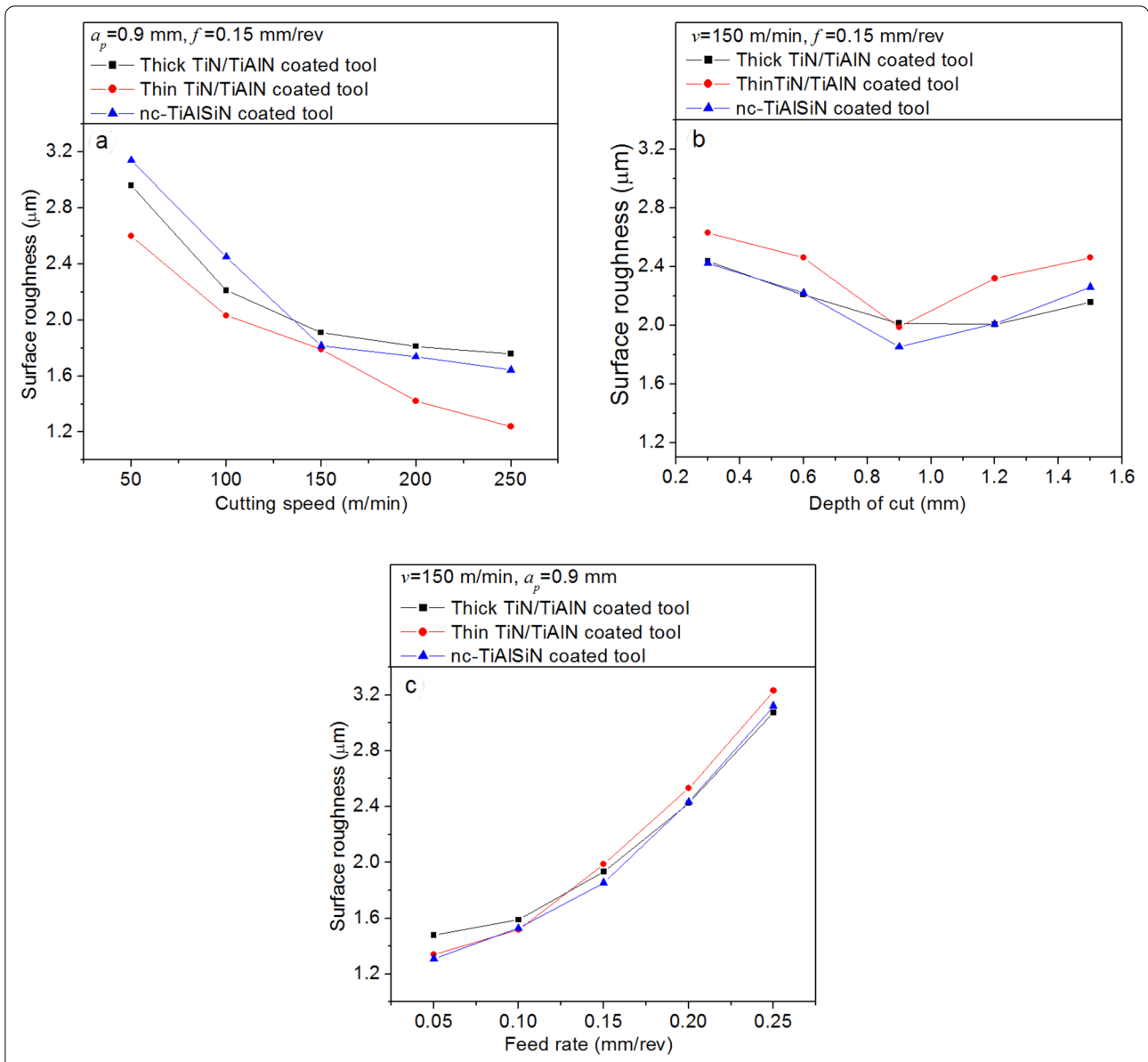
#### 4 Targeted Combinations of Cutting Conditions

Table 5 summarizes the influence of the coating materials on the cutting performances of the tools, and Table 6 relates the tool cutting parameters to the machining targets. The results highlight the importance of selecting suitable coating materials and cutting parameters for the target task. High cutting speed, low depth of cut, and low feed rate will reduce the force and temperature of cutting. In contrast, high cutting speed, high depth of cut, and high feed rate will minimize the specific cutting energy. High cutting speed, medium depth of cut, and low feed rate will minimize the surface roughness.

#### 5 Conclusions

This study investigated the influences of three PVD coating materials on the cutting performance of carbide coated tools during MCI machining under various cutting parameters. Moreover, the tool wear mechanism of MCI machining was compared with that of CGI. The conclusions are summarized below.

- (1) The nc-TiAlSiN coated tool minimized the cutting force, specific cutting energy, surface roughness, and tool wear, and maximized the tool life. Therefore, the nc-TiAlSiN coated tool is the best choice for dry cutting of MCI.
- (2) The chip shape was closely related to tool wear. During MCI machining with large cutting parameters, the chips were ejected as large blocks and the tool wear was serious. Under these conditions, the thin TiN/TiAlN coated tool exhibited more severe tool wear than the other examined tools, generating many large block chips.
- (3) Various cast irons place different demands on the cutting performance of tools. In MCI machining, the main tool-wear mechanism was adhesive wear, requiring coated tools with low affinity and low friction coefficient. In CGI machining, the main tool-wear mechanism was abrasive wear, requiring



**Figure 11** Surface roughness values of the three coated tools under various cutting conditions in dry turning of MCl: **a**  $a_p = 0.9 \text{ mm}, f = 0.15 \text{ mm/rev}$ ; **b**  $v = 150 \text{ m/min}, a_p = 0.9 \text{ mm}$  and **c**  $v = 150 \text{ m/min}, f = 0.15 \text{ mm/rev}$

**Table 5** Effect of coating materials on the cutting performances of coated tools

Coating materials	Cutting performance of coated tools				
	Cutting force	Cutting temperature	Specific cutting energy	Flank wear	Surface roughness
Thick TiN / TiAlSiN	Highest	Lowest	Highest	Higher	Higher
Thin TiN / TiAlSiN	Higher	Higher	Higher	Highest	Highest
nc-TiAlSiN	Lowest	Highest	Lowest	Lowest	Lowest

**Table 6** Relationship between machining targets and cutting parameters of different coated tools

Coated tools	Machining targets			
	Lowest cutting force	Lowest cutting temperature	Minimum specific cutting energy	Lowest surface roughness
Thick TiN/TiAlSiN coated tool	High $v$ Low $a_p$ Low $f$	High $v$ Low $a_p$ Low $f$	High $v$ High $a_p$ High $f$	High $v$ Medium $a_p$ Low $f$
Thin TiN/TiAlSiN coated tool	High $v$ Low $a_p$ Low $f$	High $v$ Low $a_p$ Low $f$	High $v$ High $a_p$ High $f$	High $v$ Medium $a_p$ Low $f$
nc-TiAlSiN coated tool	High $v$ Low $a_p$ Low $f$	High $v$ Low $a_p$ Low $f$	High $v$ High $a_p$ High $f$	High $v$ Medium $a_p$ Low $f$

coated tools with high hardness and good impact resistance.

The traditional cooling method damages the environment and human health, but alternative green cooling methods (such as liquid nitrogen, CO<sub>2</sub>, and low-temperature cold air) require costlier cooling equipment. For these reasons, the dry cutting process was adopted in the present research. In future study, we will consider the quasi dry cutting method to further improve the machining performance of coated tools.

#### Authors' Contributions

SL contributed the theoretical work and wrote the paper. HL constructed the figures and charts. TZ performed the experiments and data analysis of dry turning MCI. JS constructed the experimental equipment. CW revised the paper. All authors read and approved the final manuscript.

#### Funding

Supported by National Major Science and Technology Projects of China (Grant No. SK201901A31-04) and Key Program of NSFC-Guangdong Joint Fund, China (Grant No. U1201245).

#### Competing Interests

The authors declare that they have no conflict of interest.

#### Authors' Information

Suyang Li, born in 1974, is currently a lecture at *School of Electromechanical Engineering, Guangdong University of Technology, China*. She received her PhD degree from Nagoya University, Japan, in 2008. Her research interests include high-speed machining of difficult-to-machine materials, mechanical CAD/CAE. Haisheng Lin, born in 1989, is currently a post-doctor at *Guangdong University of Technology, China*. He received his PhD degree from Guangdong University of Technology, China, in 2014. Jianbo Sui, born in 1984, is currently an associate professor at *School of Electromechanical Engineering, Guangdong University of Technology, China*. He received his PhD degree from the University of Tokyo, Japan, in 2014. His research interests include manufacturing process modeling, machining mechanics and medical devices. Chengyong Wang, born in 1964, is currently a professor and a PhD supervisor at *Guangdong University of Technology, China*. He received his PhD degree from *Dalian University of Technology, China*, in 1989. His research interests include high

speed machining theory and CAD/CAM, high-speed machining coated tool preparation, superhard materials and tool manufacturing, etc.

#### Author Details

<sup>1</sup>School of Electromechanical Engineering, Guangdong University of Technology, Guangzhou 510006, China. <sup>2</sup>Wenshan Business Information Management School, Wenshan 530004, China.

Received: 7 March 2020 Revised: 11 January 2021 Accepted: 28 April 2021

Published online: 24 May 2021

#### References

- [1] J A G D Sousa, W F Sales, A R Machado. A review on the machining of cast irons. *The International Journal of Advanced Manufacturing Technology*, 2017, 1: 1-20.
- [2] G Ljustina, R Larsson, M Fagerstr. A FE based machining simulation methodology accounting for cast iron microstructure. *Finite Elements in Analysis & Design*, 2014, 80(2): 1-10.
- [3] V Nayyar, J Kaminski, A Kinnander, et al. An experimental investigation of machinability of graphitic cast iron grades; flake, compacted and spheroidal graphite iron in continuous machining operations. *Procedia CIRP*, 2012, 1(7): 88-493.
- [4] X M Chen, S Q Wang, D Q Yi. Development and application of insert for cutting cast iron. *Tool Engineering*, 2005, 39(5): 56-59 (in Chinese).
- [5] R Viana, D Lima, M S F Fernandes, et al. Laser texturing of substrate of coated tools - Performance during machining and in adhesion tests. *Surface & Coatings Technology*, 2015, 276: 485-501.
- [6] L Chen, J E Stahl, Z Wu, et al. Assessment on abrasiveness of high chromium cast iron material on the wear performance of PCBN cutting tools in dry machining. *Journal of Materials Processing Technology*, 2018, 255: 110-120.
- [7] V V D Oliveira, P A C Beltrão, G Pintaude. Effect of tool geometry on the wear of cemented carbide coated with TiAlN during drilling of compacted graphite iron. *Wear*, 2011, 271(9): 2561-2569.
- [8] C Y Wang, H S Lin, X Wang, et al. Effect of different oil-on-water cooling conditions on tool wear in turning of compacted graphite cast iron. *Journal of Cleaner Production*, 2017, 148: 477-489.
- [9] A G D S Jose, W F Sales, W L Guesser, et al. Machinability of rectangular bars of nodular cast iron produced by continuous casting. *The International Journal of Advanced Manufacturing Technology*, 2018, 98(9-12): 2505-2517.
- [10] S Tooptong, K H Park, P Kwon. A comparative investigation on flank wear when turning three cast irons. *Tribology International*, 2018, 120, 127-139.
- [11] R Yigit, E Celik, F Findik, et al. Tool life performance of multilayer hard coatings produced by HTCVD for machining of nodular cast iron. *International Journal of Refractory Metals and Hard Materials*, 2008, 26(6): 514-524.

- [12] I Martinez, R Tanaka, Y Yamane, et al. Wear mechanism of coated tools in the turning of ductile cast iron having wide range of tensile strength. *Precision Engineering*, 2016, 47: 46-53.
- [13] P C Jindal, A T Santhanam, U Schleinkofer, et al. Performance of PVD TiN, TiCN, and TiAlN coated cemented car-bide tools in turning. *International Journal of Refractory Metals & Hard Materials*, 1999, 17(1/2/3): 163-170.
- [14] P Fiorini, G Byrne. The influence of built-up layer formation on cutting performance of GG25 grey cast iron. *CIRP Annals - Manufacturing Technology*, 2016, 65: 93-96.
- [15] G Z Tu, S H Wu, J Liu, et al. Cutting performance and wear mechanisms of Sialon ceramic cutting tools at high speed dry turning of gray cast iron. *International Journal of Refractory Metals and Hard Materials*, 2016, 54: 330-334.
- [16] S Kurama, I Schulz, M Herrmann. Wear properties of  $\alpha$ - and  $\alpha/\beta$ -SiAlON ceramics obtained by gas pressure sintering and spark plasma sintering. *Journal of the European Ceramic Society*, 2011, 31(5): 921-930.
- [17] J Vleugels, T Laoui, K Vercammen, et al. Chemical interaction between a Sialon cutting tool and iron-based alloys. *Materials Science and Engineering: A*, 1994, 187(2): 177-182.
- [18] Y Long, J J Zeng, D H Yu, et al. Microstructure of TiAlN and CrAlN coatings and cutting performance of coated silicon nitride inserts in cast iron turning. *Ceramics International*, 2014, 40(7): 9889-9894.
- [19] S Gabaldo, A E Diniz, C L F Andrade, et al. Performance of carbide and ceramic tools in the milling of compact graphite iron-CGI. *Journal of the Brazilian Society of Mechanical Sciences and Engineering*, 2010, 32: 511-517.
- [20] M Chen, J Li, G Q Guo, et al. Experimental and FEM study of coated and uncoated tools used for dry Milling of compacted graphite cast iron. *Transactions of Tianjin University*, 2011, 17: 235-241.
- [21] I Martinez, R Tanaka, Y Yamane, et al. Wear mechanism of coated tools in the turning of ductile cast iron having wide range of tensile strength. *Precision Engineering*, 2017, 47: 46-53.
- [22] G Z Tu, S H Wu, J Liu, et al. Cutting performance and wear mechanisms of Sialon ceramic cutting tools at high speed dry turning of gray cast iron. *Int. Journal of Refractory Metals and Hard Materials*, 2016, 54: 330-334.
- [23] J Capus. A new PM route for machinable, malleable iron. *Metal Powder Report*, 2012, 67(5): 30-32.
- [24] W L Chen, T Hu, Y Hong, et al. Comparison of microstructures, mechanical and tribological properties of arc-deposited AlCrN, AlCrBN and CrBN coatings on Ti-6Al-4V alloy. *Surface & Coatings Technology*, 2020, 404: 126429.
- [25] Y H Yuan, Z Qin, D H Yu, et al. Relationship of microstructure, mechanical properties and hardened steel cutting performance of TiSiN-based nanocomposite coated tool. *Journal of Manufacturing Processes*, 2017, 28: 399-409.
- [26] X D Sui, G J Li, X S Qin, et al. Relationship of microstructure, mechanical properties and titanium cutting performance of TiAlN/TiAlSiN composite coated tool. *Ceramics International*, 2016, 42: 7524-7532.
- [27] H W Song, G Q Ren, J Q Dan, et al. Experimental study on the cutting force during laser-assisted machining of fused silica based on the Taguchi method and response surface methodology. *Journal of Manufacturing Processes*, 2019, 38: 9-20.
- [28] L R R D Silva, R Ruzzi, V Teles, et al. Analysis of the coefficient of friction at the workpiece-tool interface in milling of high strength compacted graphite cast irons. *Wear*, 2019, (426-427): 1646-1657.
- [29] N Bhopale, N Patil, S Mastuf. The experimental investigations into dry turning of austempered ductile iron. *Procedia Manufacturing*, 2018, 20: 227-232.
- [30] F Ding, C Wang, H Lin, et al. Research on machining compacted graphite iron under oil-on-water cooling and lubrication conditions based on modified material model. *The International of Advanced Manufacturing Technology*, 2019, 105(7): 5061-5079. <https://doi.org/10.1007/s00170-019-04543-y>.
- [31] R Yigit, E Celik, F Findik, et al. Effect of cutting speed on the performance of coated and uncoated cutting tools in turning nodular cast iron. *Journal of Materials Processing Technology*, 2008, 204(1-3): 80-88.
- [32] K Katuku, A Koursaris, I Sigalas. Wear, cutting forces and chip characteristics when dry turning ASTM Grade 2ADI with PcBN cutting tools under finishing conditions. *Journal of Material Processing Technology*, 2009, 209(5): 2412-2420.
- [33] F E Pfefferkorn, S Lei, Y Jeon, et al. A metric for defining the energy efficiency of thermally assisted machining. *International Journal of Machine Tools & Manufacture*, 2009, 49(5): 357-365.
- [34] A K Parida, K Maity. Numerical and experimental analysis of specific cutting energy in hot turning of Inconel 718. *Measurement*, 2019, 133: 361-369.
- [35] W Grzesik, P Nieslony. Physics based modelling of interface temperatures in machining with multilayer coated tools at moderate cutting speeds. *International Journal of Machine Tools & Manufacture*, 2004, 44(9): 889-901.
- [36] J Martan, P Benes. Thermal properties of cutting tool coatings at high temperatures. *Thermochimica Acta*, 2012, 539: 51-55.
- [37] W Grzesik. The role of coatings in controlling the cutting process when turning with coated indexable inserts. *Journal of Materials Processing Technology*, 1998, 79(1-3): 133-143.
- [38] S J Zhang, Z Q Liu. Formation of diffusion layer and its influences on heat transfer for coated tools. *International of Mechanical Engineering*, 2010, 46(21): 194-198. (in Chinese)
- [39] C Y Wang, Y X Xie, Z Qin, et al. Wear and breakage of TiAlN- and TiSiN-coated carbide tools during high-speed milling of hardened steel. *Wear*, 2015, (336-337): 29-42.
- [40] C Y Wang, Y X Xie, L J Zheng, et al. Research on the chip formation mechanism during the high-speed milling of hardened steel. *International Journal of Machine Tools & Manufacture*, 2014, 79(4): 31-48.
- [41] P Koshy, R C Dewes, D K Aspinwall. High speed end milling of hardened AISI D2 tool steel (~58 HRC). *Journal of Materials Processing Technology*, 2002, 127(2): 266-273.
- [42] G Gille, B Szesny, K Dreyer, et al. Submicron and ultrafine grained hard-metals for microdrills and metal cutting inserts. *International Journal of Refractory Metals & Hard Materials*, 2002, 20: 3-22.
- [43] S D N Rosa, A E Diniz, C L F Andrade, et al. Analysis of tool wear, surface roughness and cutting power in the turning process of compact graphite irons with different titanium content. *Journal of the Brazilian Society of Mechanical Sciences and Engineering*, 2010, 32(3): 234-240.
- [44] N Camuşcu. Effect of cutting speed on the performance of Al<sub>2</sub>O<sub>3</sub> based ceramic tools in turning nodular cast iron. *Materials & Design*, 2006, 27(10): 997-1006.
- [45] V D Patel, A H Gandhi. Analysis and modeling of surface roughness based on cutting parameters and tool nose radius in turning of AISI D2 steel using CBN tool. *Measurement*, 2019, 138: 34-38.

Submit your manuscript to a SpringerOpen<sup>®</sup> journal and benefit from:

- Convenient online submission
- Rigorous peer review
- Open access: articles freely available online
- High visibility within the field
- Retaining the copyright to your article

---

Submit your next manuscript at ► [springeropen.com](https://www.springeropen.com)